

Nodal error behind discrepancies between coupled cluster and diffusion Monte Carlo in hydrogen-bonded systems

S. Lambie¹, P. López Ríos¹, D. Kats¹, and A. Alavi^{1,2,*}

¹Max Planck Institute for Solid State Research, Heisenbergstraße 1, 70569 Stuttgart, Germany

²Yusuf Hamied Department of Chemistry, University of Cambridge, Lensfield Road, Cambridge CB2 1EW, United Kingdom

*a.alavi@fkf.mpg.de

ABSTRACT

The small magnitude and long-range character of non-covalent interactions pose a significant challenge for computational quantum chemical and electronic-structure methods alike. State-of-the-art coupled cluster (CC) theory and benchmark-grade diffusion Monte Carlo (DMC) are ideally positioned to tackle these problems, but concerning differences between both methods have been reported in numerous studies of the interaction energy of non-covalently bound dimers. Given that the basic theoretical frameworks underpinning both methods are exact in principle, the error must arise from one or several of the approximations required to make the calculations computationally tractable. Here, we carry out a rigorous and systematic examination of the effect of each of these approximations using the acetic acid dimer and water-peptide systems as convenient testing grounds. Thanks to the use of stringently optimized backflow wave functions we are able to find that the significant discrepancies are dominated by the fixed-node error incurred by the Slater-Jastrow DMC result, while errors in the CC calculations do not significantly alter the result. This finding, likely applicable to other hydrogen-bonded systems, helps establish that CC should be regarded as the benchmark for these systems, and can potentially guide the search for pragmatic solutions to the fixed-node problem in the future.

Introduction

The quality and relevance of a computational model lie in its ability to reproduce and predict experimentally observed phenomena. However, obtaining reliable experimental data which can be directly compared to computational results is a complicated and fraught endeavor, especially for non-covalent interactions. In an experiment, the effects of temperature and solvent are embedded in any measurement and must be disentangled from the measurement itself; a non-trivial process which introduces errors that are difficult to quantify. By contrast, theoretical calculations establish the interaction energy between two rigid molecules at 0 K in the gas phase, with the comparison to experiment being further exacerbated by the typically small magnitude of these interactions. High-quality quantum chemical calculations approximating the exact full configuration interaction (FCI) result in the complete basis set (CBS) limit provide crucial benchmark results to which the quality of other theoretical models can be established.

In quantum chemistry, coupled cluster (CC) theory^{1,2} has long provided a systematically improvable, hierarchical approach for moving toward the exact solution of the Schrödinger equation of molecules of moderate sizes as more excitations are included in the cluster operator. In turn, the diffusion quantum Monte Carlo (DMC) method has emerged among electronic structure methods as one of the most accurate approaches to solving the Schrödinger equation for systems with several hundreds of electrons. As computational resources have become more powerful over the past few decades, CC has become applicable to larger system sizes while DMC has seen improvements in the quality with which moderately-sized systems can be described. Comparisons of the two methods are, therefore, of great interest,^{3–6} and several recent studies in the literature have focused on disagreements found between CC and DMC in weakly-interacting systems for which DMC is expected to be particularly well-suited.^{7–9}

Both CC theory and the DMC method are, in principle, capable of exactly solving the Schrödinger equation,¹⁰ but in practice both require the use of a variety of approximations. In the case of CC theory, the cluster operator is typically truncated at the singles, doubles, and perturbative triples (CCSD(T)) level,¹¹ which provides a very good balance of accuracy and computational cost compared to CCSDT(Q) and CCSDTQ¹² for a majority of chemical properties.^{13,14} However, the use of finite basis sets and the truncation of the cluster operator introduces errors into the calculation that grow as system size increases. The DMC method requires controlled approximations, such as the use of finite time steps and walker populations,

Table 1. Interaction energy of the AcOH dimer from CC theory in kcal mol^{-1} , expressed as the 0.5CP-corrected value plus/minus half of the total CP correction except where otherwise stated. A bold typeface is used for our best CC theory AcOH dimer interaction energy with ECPs.

This work			
In text-referral	Treatment	E_{int} [kcal mol^{-1}]	
		$(\text{AcOH})_2$	Water-peptide
CCSD(T)	DF-HF/aV5Z + CCSD(T)/aV{T,Q}Z	-19.49(5)	-8.225(5)
CCSD(T*)-F12	DF-HF-F12/aV5Z + CCSD(T*)-F12/aVQZ	-19.45(8)	-8.22(4)
Co.Co.-CCSD(T)	DF-HF/aCV5Z + CCSD(T)/aCV{T,Q}Z	-19.53(1)	-8.261(3)
ECP-CCSD(T)	DF-HF/aV5Z-eCEPP + CCSD(T)/aV{T,Q}Z-eCEPP	-19.51(1)	-8.22(3)
PNO-LCCSD(T*)-F12	DF-HF-CABS/aV5Z + PNO-LCCSD(T*)-F12/aV5Z	-19.35(2)	-8.18(2)
<i>Best CC estimate</i>	HF/aCV5Z + CCSD(T)/aCV{T,Q}Z + $\Delta\text{SVD-DC-CCSDT+aVTZ}$	-19.54(1)	-8.242(3)
Best ECP CC estimate	DF-HF/aV5Z-eCEPP + CCSD(T)/aV{T,Q}Z-eCEPP+ $\Delta\text{SVD-DC-CCSDT+aVTZ}$	-19.52(1)	-8.20(3)
Reference values			
Ref. 23	HF/aV{T,Q}Z + MP2/aV{T,Q}Z + $\Delta\text{CCSD(T)/haV\{D,T\}Z}$ (CP)	-19.41	-8.22
Ref. 24	HF-CABS/V5Z-F12 + MP2-F12/aV{T,Q}Z-F12 + $\Delta\text{CCSD(F12*)/VTZ-F12 + \Delta(T)/haV\{D,T\}Z}$	-19.364(5)	-8.18(1)
Ref. 25	HF-CABS/aVQZ-F12+ MP2/aV{T,Q}Z-F12 + $\Delta\text{CCSD(*)/haV\{D,T\}Z + \Delta(T)/haV\{T,Q\}Z}$ (mixed)	-19.38	-8.19
Ref. 9	Ref. 24 + CCSD(cT)-fit (mixed)	-19.27	-8.15

and uncontrolled approximations, such as the use of pseudopotentials and the localization approximation they require. However, the bulk of the error incurred by DMC is ultimately from the fixed-node approximation, whereby the DMC energy depends on the quality of the nodes of a trial wave function that guides the stochastic sampling process.

The finding of significant discrepancies between the two methods for non-covalent interaction energies^{7,8} stimulated a flurry of additional studies investigating the possible sources of disagreement.¹⁵⁻²¹ The issue was initially thought to be restricted to large, dispersion-bound systems, but substantial deviations were also found for small H-bound systems.⁹ To date, the origin of the discrepancy between the two state-of-the-art methods has not been definitively identified. Here, we focus on the two case-study examples of the 16-atom acetic acid (AcOH) dimer and 15-atom water-peptide system, corresponding to systems 20 and 4 of the hydrogen-bonded portion of the S66 set, respectively;²² see insets in Fig. 1. For the AcOH dimer, a discrepancy of about 0.8 kcal mol^{-1} has been reported between the DMC value of $-20.17(7)$ kcal mol^{-1} and canonical CC value of $-19.39(2)$ kcal mol^{-1} ,⁹ while for the water-peptide system, the difference between the DMC result of $-8.58(7)$ kcal mol^{-1} and the CC result of $-8.20(2)$ kcal mol^{-1} is about 0.4 kcal mol^{-1} .⁹ The AcOH dimer and water-peptide systems thus provide a wonderful opportunity for probing sources of error between the two methods thanks to the large energy discrepancies and small system sizes.

1 Coupled cluster results

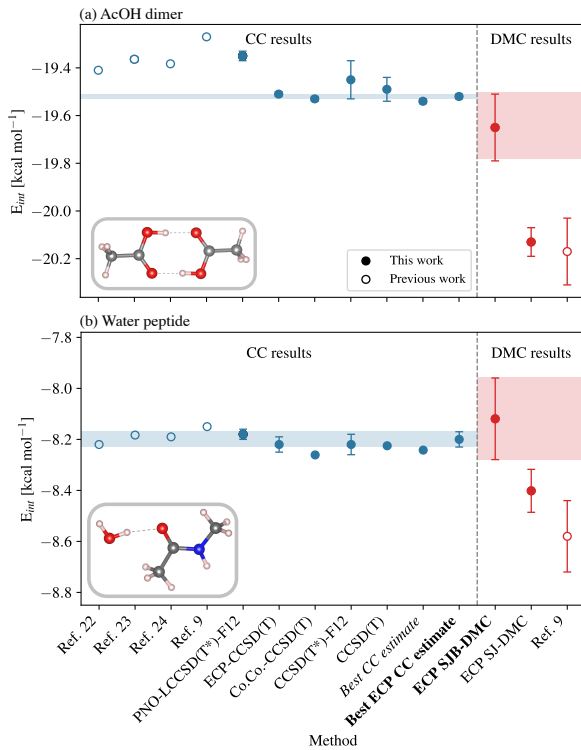


Figure 1. Interaction energy of (a) the AcOH dimer and (b) the water-peptide dimer obtained using CC theory (blue) and DMC (red). The interaction energies that allow for the most direct comparison between each methodology (bold) with a ‘two-sigma’ confidence interval are shown as a shaded area. For the CC calculations, 0.5CP-corrected values are reported with non-statistical error bars extending from the CP-uncorrected to the CP-corrected result; note that reference CC values are plotted as single points. The error bars on the DMC values are purely statistical in nature, representing 95% (two-sigma) confidence intervals, and include optimization uncertainty where pertinent, see text. The insets show the structures considered with C atoms in grey, O atoms in red, H atoms in pink and N atoms in blue.

In CC theory, ‘gold standard’ results are obtained by truncating the CC operator at the CCSD(T) level, which provides an excellent balance of accuracy and computational cost due to a systematic cancellation of errors.^{13,14,26} However, a beyond-‘gold’ standard is required for benchmarking quantum chemical methods, taking into consideration all possible sources of error in CCSD(T). We have studied the convergence of CC results with respect to the basis set (section 1.1), electronic excitations (section 1.2), local implementation (section 1.3), and CC operator (section 1.4).

1.1 Approaching the complete basis set limit

All basis sets are finite and, as a result, incomplete, meaning that both basis set superposition error (BSSE)²⁷ and basis set incompleteness error (BSIE)²⁸ require careful management. The counterpoise (CP) correction is the most common approach for dealing with BSSE,²⁹ which allows the CBS limit to be approached more smoothly and quickly than with uncorrected (raw) values.^{30,31} Raw and CP-corrected results typically provide a lower and upper bound, respectively, for the CBS value, within a specific CC operator truncation,³¹ and for this reason we report our CC results as the arithmetic mean of the raw and CP-corrected values plus/minus a half of the full CP correction, so that the ‘two-sigma’ interval, which corresponds to the 95% confidence interval for statistical standard errors, covers the full CP range. This simplifies comparison with DMC where error bars occur naturally, but bear in mind that our CC ‘error bars’ are not statistical in nature. In the CBS limit, both the BSIE and BSSE vanish, along with the need for CP corrections.

Correlation energy is slowly convergent with basis-set size,^{32–36} and basis sets of at least augmented triple zeta (aVTZ) size are essential for CC results to be considered reliable for non-covalent interactions.³⁷ For this reason, the largest computationally-affordable basis sets are used in conjunction with techniques to approximate the CBS limit, such as focal-point (FP) approaches,^{31,38} CBS extrapolations^{30,34} and explicitly correlated F12 methods.³⁹

FP approaches^{31,38} exploit the fact that the total energy of a post-Hartree-Fock method can be decomposed into the Hartree-Fock (HF) component and various correlation energy contributions calculated using basis sets of different sizes, taking advantage of the fact that the energy offset between methods is fairly consistent. The FP approach can then be coupled further with a CBS extrapolation,^{30,34} so that the correlation energy component of the calculation can be obtained in smaller basis sets and extrapolated to the CBS limit. Explicitly correlated methods significantly improve basis set convergence by including geminal functions that rely on the inter-electronic distance into the wavefunction ansatz.^{39,40} The (T) treatment does not contain any F12 terms⁴¹ and, therefore, the (T) energy must be scaled (see Section 3) resulting in the CCSD(T*)-F12 method. Performance of CCSD(T*)-F12 with aVTZ and aVQZ basis sets is known to be comparable to CBS extrapolated canonical CCSD(T)/aV{Q,5}Z results for non-covalent interactions.⁴² Here, the CCSD(T*)-F12 results agree with the CCSD(T) results (Table 1), to which it can be most directly compared, determining that both the explicitly correlated method and CBS extrapolated results converge toward the CBS limit for the interaction energy of the AcOH dimer and water-peptide system at the CCSD(T) level of theory. For the AcOH dimer, we additionally test the truncated heavy-atom only augmented⁴³ and density fitted^{44,45} basis sets with minimal changes to the results, see Section S1 of the supplementary information.

In general, we find that our CC results for the AcOH dimer and the water-peptide system are in good agreement with the literature (Table 1).^{23–25} However, the results of the present study can be expected to be more accurate than previously reported values thanks, in part, to our use of larger basis sets. Additionally, the previously reported values use the FP approach extensively – that is, they make two key assumptions that could introduce an undefined error into the results. Firstly, all reference values assume that the difference in energy between lower order methods, such as MP2 and CCSD(T) is constant and unchanging as the size of the basis set is increased. Secondly, they assume that these energetic differences are converged in small basis sets, such as the heavy-atom augmented double-triple-zeta extrapolation Δ CCSD(T) energetic correction, used in Ref 23. While the FP approach is generally applicable, and introduces small errors, these errors are not necessarily systematic³¹ and are relevant on the scale of interest for the non-covalent interactions reported in the present study. As such, it is imperative to control all sources of error in the coupled cluster calculations and by calculating the correlation energy in large basis sets with minimal usage of the FP approach, we control these additional sources of error in the present calculations. It should also be noted that some of the previous studies referenced here reported individual interaction energies containing a specific amount of CP correction, and are therefore comparable with the outer limits of our ‘two-sigma’ confidence intervals.

1.2 Core electron treatments

The frozen core approximation is routinely used in CC calculations, but its effect on the results is rarely considered. In the present study, calculations invoke the frozen core approximation unless otherwise stated. Alternative treatments of the core region exist, in particular, the explicit inclusion of core correlation in the calculation (Co.-Co.-CCSD(T)) through the use of correlation consistent core-valence basis sets, aCVX Z, X = T, Q, where the C indicates that the basis set is suitable for correlating core electrons,⁴⁶ or the core can be treated using effective core potentials (ECP-CCSD(T)), as commonly used in DMC calculations; specifically, we use energy-consistent correlated electron pseudopotentials (eCEPPs).⁴⁷

We have performed calculations of the AcOH dimer and water-peptide system with all three treatments of the core, and we find that a very small stabilisation on the order of 0.04 kcal mol⁻¹ arises as a result of including core correlation in the calculation. Therefore, we conclude that core treatment is unlikely to be responsible for the significant discrepancy between the CC and DMC results.

1.3 Local coupled cluster

Local methods^{48–50} are designed to reach larger system sizes with high accuracy and are often used to obtain CCSD(T)/CBS reference values for non-covalent interaction energies of large molecules.^{7,8,21,51,52} Here, we focus on the most accurate of the local methods, PNO-LCCSD(T*)-F12,⁵⁰ where the combination of local and scaled F12 methods is highly effective at reducing the basis-set and domain errors.^{50,53–55} However, both basis set and local errors increase as the system size grows,^{50,56} and, therefore, the fidelity of local methods to the canonical result is expected to deteriorate with increasing system size.^{50,52} While the reduced scaling offered by local methods is not required to simulate the systems considered in this study due to their small size, we test this method for its performance compared to the canonical result to better understand possible sources of error.

The PNO-LCCSD(T*)-F12 calculations are a small underestimation of the CCSD(T*)-F12 results (Table 1), as expected by the method developers.^{50,57} While the low basis-set error of local methods^{58–61} would appear to indicate a low error on local CC values, we advise that confidence intervals be estimated conservatively for local calculations, extending beyond basis-set error, until the extrapolation of local results to the canonical limit is well-established.⁶²

1.4 Beyond gold standard coupled cluster

For molecular dimers it has been found that CCSD(T) regularly outperforms CCSDT,^{13,14,20,63,64} and that CCSDT(Q) and CCSDTQ typically produce results that are converged with respect to the cluster operator for non-covalent interactions.¹³

Table 2. DMC interaction energy of the AcOH dimer and the water-peptide system, in kcal mol⁻¹. Uncertainties shown represent 95% (2-sigma) confidence intervals. A bold typeface is used for our best DMC interaction energy.

Method	This work	
	E _{int} [kcal mol ⁻¹] (AcOH) ₂	Water-peptide
AE SJ-DMC	-20.29(16)	-
ECP SJ-DMC	-20.13(6)	-8.40(8)
ECP SJ-B-DMC	-19.65(14)	-8.12(16)
Reference values		
ECP SJ-DMC ⁹	-20.17(14)	-8.58(14)

However, the perturbative treatment of excitations in CC theory causes diverging results in the metallic limit.^{17,19,65} Since the discrepancy between DMC and CC results was first reported for increasingly large dispersion-bound C-based molecules⁷⁻⁹ with diminishing HOMO-LUMO gaps,⁶⁶⁻⁶⁸ lack of convergence with respect to the truncation of the CC operator must be considered as a possible source of error.

Even for the small systems considered in this study, the N^9 scaling of CCSDT(Q) means that canonical calculations in large basis sets are unattainable. Therefore, post-CCSD(T) corrections can be obtained by approximating the CC operator through the use of CCSD(cT)¹⁹ or rank-reduced distinguishable cluster (SVD-DC-CCSDT+)⁶⁹⁻⁷² methods, or by using very small, truncated basis sets to carry out canonical CCSDT(Q) calculations.⁶⁴

Each of these approaches has its own limitations. CCSD(cT)¹⁹ approximates CCSDT, which is known to be somewhat inaccurate for non-covalent interactions.^{13,14,20,63,64} SVD-DC-CCSDT+⁶⁹ enables larger basis sets to be used but is a new method that has currently only been benchmarked to the A24 dataset.^{73,74} Additional benchmarking of the SVD-DC-CCSDT+ method for the AcOH dimer and water-peptide system is shown in the supplementary information. Canonical CCSDT(Q) results⁶⁴ require the use of small basis sets, implying that these corrections cannot be expected to be converged with respect to basis set size.⁷⁵ Nevertheless, these three approaches result in small post-CCSD(T) corrections of, for the AcOH dimer 0.12 kcal mol⁻¹, -0.01 kcal mol⁻¹ and 0.055 kcal mol⁻¹, and for the water-peptide system of 0.05 kcal mol⁻¹, 0.019 kcal mol⁻¹ and 0.012 kcal mol⁻¹, respectively, for fitted CCSD(cT),⁹ SVD-DC-CCSDT+/aVTZ, and CCSDT(Q)/VDZ(d,s).⁶⁴ Interestingly, all of the results considering higher order excitations in the cluster operator than CCSD(T) have either negligible effects or reduce the magnitude of the CC result, thereby increasing the discrepancy between the DMC and CC results. We, therefore, conclude that the discrepancy with DMC is highly unlikely to be sourced from truncation of the CC operator.

1.5 Other considerations and the best coupled cluster estimate

Our best CC estimates for the interaction energy of the AcOH dimer and water-peptide system using CC-based methodologies are -19.54(1) kcal mol⁻¹ and -8.242(3) kcal mol⁻¹, respectively. These calculations improve upon previously reported values by using larger basis sets for the correlation energy component of the calculations, considering excitations from the deep core and an approximate post CCSD(T) correction. Other possible sources of error in our best estimate could arise from scalar relativistic effects and diagonal Born-Oppenheimer corrections, however, these are known to be negligibly small for light atoms,⁷⁶ such as C, N, O, and H found in (AcOH)₂ and the water-peptide system, and are also absent from the DMC calculations.

Since none of the approximations employed in CC theory are able to explain the discrepancy with the DMC results, we turn to examining possible sources of error arising from the approximations involved in the DMC calculations. To directly compare between CC and DMC, we take the ECP-CCSD(T) result and add a post-CCSD(T) correction to obtain our ‘best ECP CC estimate.’

2 Diffusion quantum Monte Carlo results

2.1 Slater-Jastrow results

We have run DMC calculations of the AcOH, (AcOH)₂, water, peptide, and water-peptide systems using the Slater-Jastrow (SJ) trial wave function and ECPs to represent ionic cores, namely eCEPPs,⁴⁷ with which we recover ECP SJ-DMC results within uncertainty of those reported in Ref. 9, see Table 2 and Fig. 1.

There are various potential sources of error in the DMC results. DMC calculations are performed at finite time steps τ , and the resulting energies must be extrapolated to zero time step as we report in Section S2 the supplementary information. Population control bias is typically negligible and can be removed by extrapolation along with time-step bias,⁷⁷ which we

have done. We have verified that the error incurred by the use of ECPs is negligible on the scale of interest by computing the all-electron (AE) SJ-DMC interaction energy of the AcOH dimer, reported in Table 2, which agrees within uncertainty with its ECP counterpart. We have tested using distinct Jastrow parameters for symmetry-inequivalent atoms,⁷⁸ but we find that this does not change the interaction energy estimate for (AcOH)₂. The source of the remaining error in DMC is the mismatch between the nodes of the trial wave function and those of the exact wave function, which is referred to as the fixed-node error. Note that BSIE can be regarded as part of the fixed-node error in DMC; our use of the relatively large aug-cc-pVTZ basis set should provide a good starting point for this source of fixed-node error.

2.2 Beyond Slater-Jastrow nodes: backflow results

The use of multideterminant expansions is a popular approach for obtaining beyond-SJ nodes to study electronic excitations of small molecules,^{79–89} but it suffers from significant size-consistency issues that preclude the calculation of accurate interaction energies, especially for the system sizes of interest here, so we have instead chosen to apply backflow^{90–94} to Ψ_S . In the Slater-Jastrow-backflow (SJB) wave function the arguments of the single-particle orbitals are replaced with quasiparticle coordinates that depend on the positions of all other electrons, smoothly altering the shape of the SJ nodal surface; see Section S2 of the supplementary information for further details. SJB-DMC is often capable of removing about half of the fixed-node error in the SJ-DMC energy.^{77,80,81} The use of backflow incurs a significant increase in the computational cost of DMC calculations, so it is typically not used for large systems, but the expense is manageable for the systems studied here when ECPs are used. The topical, very flexible neural-network wave functions^{95,96} incorporate Jastrow-, backflow-, orbital-, and multideterminant-like degrees of freedom, but we have opted against using these because they incur potentially greater costs, require specialized workflows and hardware, and preclude straightforward comparisons with SJ-DMC.

VMC-based optimization of Jastrow factors is usually performed without considering the presence of statistical uncertainties on the resulting parameters arising from the stochastic nature of the optimization process. This is because the Jastrow factor parameters in the SJ wave function do not affect the value of (all-electron) SJ-DMC energies at $\tau = 0$, but there are scenarios where wave function parameters significantly affect expectation values,^{97–99} as is the case of the DMC energy in the presence of backflow. Ignoring optimization uncertainty can thus result in the perception that SJB-DMC energies behave erratically and are inconsistent across systems.

The optimization uncertainty on the SJB-DMC energy σ_{opt} depends on the number of real-space configurations n_{opt} used in VMC-based correlated-sampling optimization via $\sigma_{\text{opt}}^2 = \alpha/n_{\text{opt}}$, where α is a system-dependent unknown, at sufficiently large n_{opt} , see section S2 of the supplementary information. For a given n_{opt} , the optimization uncertainty on the SJB-DMC energy can be evaluated by running multiple independent random instances of optimization at that sample size, each followed by a SJB-DMC run. It is therefore possible to perform this procedure at a trial value of n_{opt} to obtain σ_{opt} in order to determine α , and thus be able to identify the value of n_{opt} necessary to obtain any given target accuracy.

To verify that the relationship between σ_{opt} and n_{opt} is applicable in practice, we have computed the optimization uncertainty on the SJB-DMC energy of the AcOH monomer, $\sigma_{\text{opt}}^{\text{AcOH}}$, for several values of n_{opt} . In Fig. 2(a) the energies from individual instances of optimization at each sample size are shown, and Fig. 2(b) is a log-log plot of $\sigma_{\text{opt}}^{\text{AcOH}}$ as a function n_{opt} , which confirms that the optimization uncertainty remains proportional to $n_{\text{opt}}^{-1/2}$ in the entire range of n_{opt} tested.

Using the average value of α obtained from these data, we pick a final optimization sample size of $n_{\text{opt}}^{\text{AcOH}} = n_{\text{opt}}^{(\text{AcOH})_2} = 10^7$ to achieve a target optimization uncertainty on the interaction energy of $\sigma_{\text{opt}} = 0.071 \text{ kcal mol}^{-1}$, set so as to obtain a total uncertainty on the interaction energy below 0.10 kcal mol⁻¹, see Fig. 2(b); note that $\sigma_{\text{opt}}^{\text{AcOH}} = \sigma_{\text{opt}}/\sqrt{6} \approx 0.029 \text{ kcal mol}^{-1}$, as discussed in section S2 of the supplementary information.

For the heterogeneous water-peptide system we choose to split the target optimization uncertainty of $\sigma_{\text{opt}} = 0.071 \text{ kcal mol}^{-1}$ in proportion to the square root of the number of electrons in each of the systems, to keep it in line with the stochastic uncertainty, and thus arrive at $\sigma_{\text{opt}}^{\text{water}} = 0.023 \text{ kcal mol}^{-1}$, $\sigma_{\text{opt}}^{\text{peptide}} = 0.045 \text{ kcal mol}^{-1}$, and $\sigma_{\text{opt}}^{\text{w-p.}} = 0.050 \text{ kcal mol}^{-1}$. In this case, we evaluate the optimization uncertainty at a single value of $n_{\text{opt}} = 3 \times 10^4$, and we thus determine target optimization sample sizes of $n_{\text{opt}}^{\text{water}} = 1.1 \times 10^7$, $n_{\text{opt}}^{\text{peptide}} = 10^6$ and $n_{\text{opt}}^{\text{w-p.}} = 7.5 \times 10^6$.

Our final SJB-DMC interaction energies of $-19.65(14) \text{ kcal mol}^{-1}$ for (AcOH)₂ and $-8.12(16) \text{ kcal mol}^{-1}$ for water-peptide, given in Table 2 and plotted in Fig. 1, are in excellent agreement with our best ECP CC energy estimates of $-19.52(1) \text{ kcal mol}^{-1}$ and $-8.20(3) \text{ kcal mol}^{-1}$, respectively, strongly supporting the hypothesis that the main cause of the disagreement between CC and SJ-DMC results in H-bonded systems is the fixed-node error.

Discussion

We have considered various potential sources of error in CC and DMC calculations of the AcOH dimer and water-peptide system, and find that the lifting of various approximations does not significantly alter the CCSD(T) result.

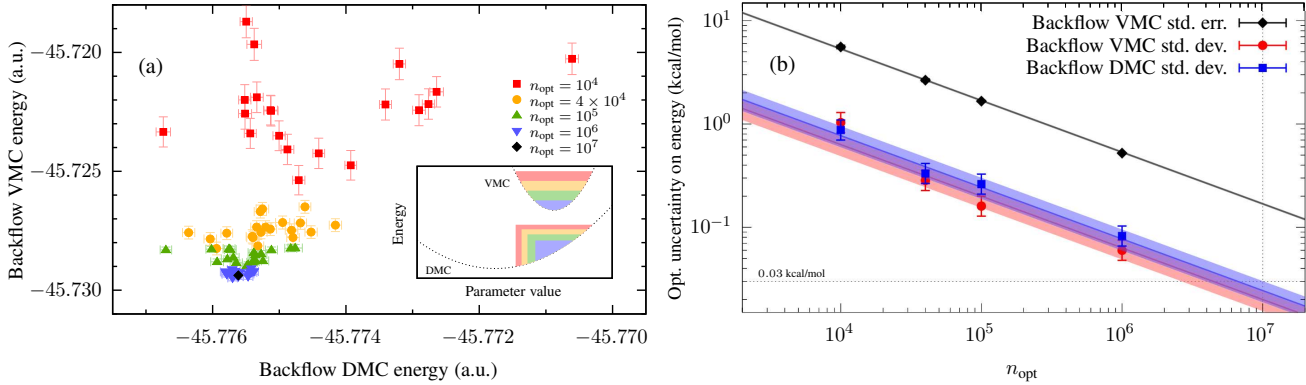


Figure 2. (a) Scatter plot of the SJB-VMC energy as a function of SJB-DMC energy of the ECP AcOH monomer for 20 independent random instances of wave function optimization at each of four optimization sample sizes n_{opt} , and for the final optimization performed at $n_{\text{opt}} = 10^7$; note the lack of visible correlation between VMC and DMC energies and the evident mismatch of the location of the VMC and DMC energy minima, schematically represented in the inset. (b) Resulting uncertainty (1-sigma confidence interval) on the SJB-VMC and SJB-DMC energy arising from the stochastic nature of optimization as a function of n_{opt} , computed as the standard deviation of the corresponding energies in Fig. 2(a), in log-log scale. The target optimization uncertainty and chosen sample size are shown as dotted lines, and solid lines are linear fits in log-log scale to the data points using a fixed slope of $-1/2$. Shaded areas and errorbars represent 95% (two-sigma) confidence intervals. Also shown is the (average) standard error on the mean value of the n_{opt} local energies used in optimization, which is an order of magnitude greater than the optimization uncertainty on the backflow VMC energy: correlated-sampling optimizers can determine the location of the energy minimum to much better accuracy than the statistical resolution of the local energy sample mean would suggest.

In both of the case-study examples considered in this work, the use of backflow brings the magnitude of the DMC interaction energy towards the CC result, in such way that the two methods are now in concordance with one another. From this we come to the conclusion that the fixed-node error in the SJ-DMC calculations is responsible for the vast majority of the disagreement between the methods reported in the literature for this class of systems. This implies that the inconsistencies in the nodes of the HF wave function (which the SJ wave function inherits) between monomer and dimer, while arguably small given the weakness of the interaction, suffice to put DMC at a disadvantage with respect to CC. The application of backflow will undoubtedly be crucial in resolving the discrepancies between CC and DMC in dispersion-bound systems too.

In order to obtain meaningful backflow results we have given explicit consideration to the uncertainty introduced by the stochastic nature of the optimization process, which accounts for the largest share of the uncertainty on our final result. Establishing the magnitude of this optimization uncertainty is crucial in ensuring that DMC energies obtained using trial wave functions with stochastically-optimized nodes are well-defined quantities not affected by uncontrolled noise.

Using backflow in the way we have in our present work is not necessarily a practical or affordable solution to the fixed-node error problem of SJ-DMC. Our SJB-DMC calculations have used 2.9 million core-hours on an AMD EPYC cluster to obtain the interaction energy of $(\text{AcOH})_2$, and 1.5 million for the water-peptide system, while their SJ-DMC counterparts cost 0.42 and 0.27 million core-hours, respectively. On top of this, we have used an unrefined approach with conservative choices of run parameters to establish the optimal value of n_{opt} , adding 1.2 and 3.4 million core-hours to the cost of the $(\text{AcOH})_2$ and water-peptide calculations, respectively. Despite its costliness, the backflow ansatz is trivially size consistent, unlike multideterminant expansions, and the optimization protocol proposed in the present work prevents this property from being adversely affected by the stochastic optimization process. This approach allows backflow to be deployed in cases where beyond-SJ nodes are important, prompting further work to make the use and optimization of backflow more affordable in practice.

3 Computational details

In keeping with previous works, we utilize the S66 geometries²² for the AcOH dimer (system 20) and the water-peptide system (system 4) throughout the study, as available from the Benchmark Energy and Geometry Database,¹⁰⁰ see Section S4 of the supplementary information.

When calculating the interaction energy, no relaxation effect of the monomers is taken into account. Intermolecular energies are calculated with the super-molecular approach; for the AcOH dimer as:

$$E_{\text{int}} = E_{\text{dimer}} - 2\dot{E}_{\text{monomer}}, \quad (1)$$

and for the water-peptide system as:

$$E_{\text{int}} = E_{\text{dimer}} - E_{\text{monomer 1}} - E_{\text{monomer 2}}. \quad (2)$$

3.1 Canonical CC calculations

CCSD(T) calculations were carried out in Molpro 2022.3.^{101,102}

CBS extrapolations are calculated using the form of Helgaker³⁰ and Halkier,³⁰ as follows:

$$E(XY) = \frac{(X^3 E_X - Y^3 E_Y)}{X^3 - Y^3} \quad (3)$$

where X and Y describe the cardinal number of the basis set and E_X and E_Y are the total correlation energies in each basis set, respectively. Basis sets employed are the augmented correlation consistent Dunning¹⁰³ aug-cc-pVXZ basis sets with $X=T, Q$, or 5 abbreviated to aVXZ. The aVTZ and aVQZ extrapolation is, for example, then denoted as aV{T, Q}Z. Basis set extrapolations are only carried out on the correlation energy which are more slowly convergent with BS size while the HF energy is not extrapolated due to its faster convergence with BS size.^{30,34} Where density fitting is employed, JKFIT⁴⁴ and MPFIT⁴⁵ of the same cardinal number as the atomic orbital basis set are used.

For the explicitly correlated calculations, the F12b explicit correlation method^{39,40} is used as it systematically converges to the CBS limit.³⁹ The scaling of the (T) energy is carried out as:

$$E_{(T^*)} = E_{(T)} \frac{E_{\text{MP2-F12}}}{E_{\text{MP2}}} \quad (4)$$

where all energies are correlation energies, of (T), MP2 and MP2-F12 to, ultimately, give a (T*) correlation energy. The scaling factor of the dimer is used for the monomer scaling in both the raw and CP corrected calculations to ensure consistency between calculations and in keeping with previous recommendations.⁵⁰ It is unclear how these methods should be extrapolated to the CBS limit and, therefore, no basis set extrapolations are carried out for either the canonical or local explicitly correlated methods.

For the Co.Co.-CCSD(T) calculations, the core region was set to zero and the core-correlated correlation consistent basis sets, aug-cc-pCVXZ,⁴⁶ were used. For the ECP-CCSD(T) calculations, the energy-consistent correlated electron pseudopotentials (eCEPPs) of Trail and Needs were employed.⁴⁷

3.2 PNO-LCCSD(T*)-F12b

Local CC calculations were carried out using (T*) scaled, explicitly correlated pair natural orbital local CCSD(T) (PNO-LCCSD(T*)-F12b).^{57,101,102} Tight domain and pair thresholds^{50,104} are used and complete auxiliary basis sets (CABS) corrections^{39,40} of the HF energy are utilized. The energy threshold for the local CCSD pair natural orbital domains was set to 0.997, as recommended for intermolecular interactions.

3.3 SVD-DC-CCSDT+

The SVD-DC-CCSDT+^{69-72,105,106} method is an approximation to CC theory that uses the distinguishable cluster approximation to remove selected exchange terms from the CC amplitude equations combined with an SVD treatment of the cluster amplitudes.¹⁰⁷⁻¹⁰⁹ SVD-DC-CCSDT+ calculations are carried out in ElemCo.jl.¹¹⁰

An SVD amplitude threshold of 10^{-6} was used in conjunction with the SVD-(T) correction scheme, as described in Ref. 74 to obtain the SVD-DC-CCSDT+ energies. Importantly, the SVD-DC-CCSDT+ method is used to obtain a post CCSD(T) correction to the energy in the aVTZ basis set, calculated within the frozen core approximation as:

$$\Delta\text{SVD-DC-CCSDT+}/\text{aVTZ} = E_{\text{corr.}}(\text{SVD-DC-CCSDT+}/\text{aVTZ}) - E_{\text{corr.}}(\text{CCSD(T)}/\text{aVTZ}). \quad (5)$$

3.4 DMC calculations

Wave function optimization and DMC runs have been performed using the CASINO code.⁷⁷ Within DMC we handle the eCEPPs⁴⁷ using the T-move scheme^{111,112} as DMC localization approximation, and we use the size-consistent local-energy limiting Green's function modifications of Zen *et al.*¹¹³ to enable accurate, efficient extrapolations to zero time step.^{114,115} Note that, by contrast with the calculations reported in Ref. 9, the single-particle orbitals in our SJ wave function are Gaussian expansions of HF orbitals using the aug-cc-pVTZ basis set¹⁰³ instead of B-spline¹¹⁶ re-expansions of local-density-approximation or Perdew-Burke-Ernzerhof plane-wave orbitals, which we cusp-correct in AE calculations,¹¹⁷ and we optimize our Jastrow^{118,119} and backflow⁹⁴ parameters using linear least-squares energy minimization^{120,121} instead of unreweighted variance minimization.¹²² Further details are reported in section S2 of the supplementary information.

Data availability

The authors declare that all data supporting the findings of this study are included in the paper and are available within the paper and its supplementary information files. Additional data is available upon reasonable request from the authors.

References

1. Čížek, J. On the correlation problem in atomic and molecular systems. Calculation of wavefunction components in Ursell-type expansion using quantum-field theory methods. *J. Chem. Phys.* **45**, 4256–4266 (1966).
2. Paldus, J., Čížek, J. & Shavitt, I. Correlation problems in atomic and molecular systems. IV. Extended coupled-pair many-electron theory and its application to the BH_3 molecule. *Phys. Rev. A* **5**, 50–67 (1972).
3. Maten, S. & Lüchow, A. On the accuracy of the fixed-node diffusion quantum Monte Carlo method. *J. Chem. Phys.* **115**, 5362–5366 (2001).
4. Mella, M. & Anderson, J. B. A brute force test of accuracies for He_2 and He-LiH . *J. Chem. Phys.* **119**, 8225–8228 (2003).
5. Dubecký, M. *et al.* Quantum Monte Carlo for noncovalent interactions: An efficient protocol attaining benchmark accuracy. *Phys. Chem. Chem. Phys.* **16**, 20915–20923 (2014).
6. Dubecký, M. *et al.* Quantum Monte Carlo describe noncovalent interactions with subchemical accuracy. *J. Chem. Theory Comput.* **9**, 4287–4292 (2013).
7. Al-Hamdani, Y. S. *et al.* Interactions between large molecules pose a puzzle for reference quantum mechanical methods. *Nat. Commun.* **12**, 3297 (2021).
8. Villot, C., Ballesteros, F., Wang, D. & Lao, K. U. Coupled cluster benchmarking of large noncovalent complexes in L7 and S12L as well as the C_{60} dimer, DNA-ellipticine and HIV-indinavir. *J. Phys. Chem. A* **126**, 4326–4341 (2022).
9. Shi, B. X. *et al.* Systematic discrepancies between reference methods for non-covalent interactions within the S66 dataset. *J. Chem. Phys.* **162**, 144107 (2025).
10. Witte, J., Goldey, M., Neaton, J. B. & Head-Gordon, M. Beyond energetics: Geometries of nonbonded molecular complexes as metrics for assessing electronic structure approaches. *J. Chem. Theory Comput.* **11**, 1481–1492 (2015).
11. Raghavachari, K., Trucks, G. W., Pople, J. A. & Head-Gordon, M. A fifth-order perturbation comparison of electron correlation theories. *Chem. Phys. Lett.* **157**, 479–483 (1989).
12. Kállay, M. & Gauss, J. Approximate treatment of higher excitations in coupled-cluster theory. *J. Chem. Phys.* **123**, 214105 (2005).
13. Řezáč, J., Šimová, L. & Hobza, P. CCSD[T] describes noncovalent interactions better than the CCSD(T), CCSD(TQ) and CCSDT methods. *J. Chem. Theory Comput.* **9**, 346–369 (2013).
14. Řezáč, J. & Hobza, P. Describing noncovalent interactions beyond the common approximations: How accurate is the “gold standard” CCSD(T) at the complete basis set limit? *J. Chem. Theory Comput.* **9**, 2151–2155 (2013).
15. Nakano, K., Sorella, S., Alfé, D. & Zen, A. Beyond single-reference fixed-node approximation in *ab initio* diffusion Monte Carlo using antisymmetrised geminal power applied to systems with hundreds of electrons. *J. Chem. Theory Comput.* **20**, 4591–4604 (2024).
16. Nakano, K., Shi, B. X., Alfé, D. & Zen, A. Basis set incompleteness errors in fixed-node diffusion Monte Carlo calculations on non-covalent interactions. *J. Chem. Theory Comput.* **21**, 4426–4434 (2025).
17. Benali, A., Shin, H. & Heinonen, O. Quantum Monte Carlo benchmarking of large noncovalent complexes in the L7 benchmark set. *J. Chem. Phys.* **153**, 194113 (2020).

18. Gray, M. & Herbert, J. M. Assessing the domain-based local pair natural orbital (DLPNO) approximation for non-covalent interactions in sizable supramolecular complexes. *J. Chem. Phys.* **161**, 054114 (2024).

19. Schäfer, T., Irmler, A., Gallo, A. & Grüneis, A. Understanding discrepancies of wavefunction theories for large molecules. *ArXiv* (2024).

20. Lambie, S., Kats, D., Usyat, D. & Alavi, A. On the applicability of CCSD(T) for dispersion interactions in large conjugated systems. *J. Chem. Phys.* **162**, 114112 (2024).

21. Lao, K. U. Canonical coupled cluster binding benchmark for nanoscale noncovalent complexes at the hundred-atom scale. *J. Chem. Phys.* **161**, 234103 (2024).

22. Řezáč, J., Riley, K. E. & Hobza, P. S66: A well-balanced database of benchmark interaction energies relevant to biomolecular structures. *J. Chem. Theory Comput.* **7**, 2427–2438 (2011).

23. Řezáč, J., Riley, K. E. & Hobza, P. Extensions of the S66 data set: More accurate interaction energies and angular displaced nonequilibrium geometries. *J. Chem. Theory Comput.* **7**, 3466–3470 (2011).

24. Kesharwani, M. K., Karton, A., Sylvetsky, N. & Martin, J. M. L. The S66 non-covalent interactions benchmark reconsidered using explicitly correlated methods near the basis set limit. *Aust. J. Chem.* **71**, 238–248 (2017).

25. Nagy, P. R., Gyevi-Nagy, L., Lörincz, B. D. & Kállay, M. Pursuing the basis set limit of CCSD(T) non-covalent interaction energies for medium-sized complexes: Case study on the S66 compilation. *Mol. Phys.* **121**, e2109526 (2022).

26. Helgaker, T., Ruden, T. A., Jørgensen, P., Olsen, J. & Klopper, W. *A priori* calculation of molecular properties to chemical accuracy. *J. Phys. Org. Chem.* **17**, 913–933 (2004).

27. Liu, B. & McLean, A. D. Accurate calculation of the attractive interaction of two ground state helium atoms. *J. Chem. Phys.* **59**, 4557–4558 (1973).

28. Davidson, E. R. & Feller, D. Basis set selection for molecular calculations. *Chem. Rev.* **86**, 681–696 (1986).

29. Boys, S. F. & Bernardi, F. The calculation of small molecular interactions by the differences of separate total energies. Some procedures with reduced errors. *Mol. Phys.* **19**, 553–566 (1970).

30. Halkier, A., Klopper, W., Helgaker, T., Jørgensen, P. & Taylor, P. R. Basis set convergence of the interaction energy of hydrogen-bonded complexes. *J. Chem. Phys.* **111**, 9157–9267 (1999).

31. Burns, L. A., Marshall, M. S. & Sherrill, C. D. Comparing counterpoise-corrected, uncorrected, and averaged binding energies for benchmarking noncovalent interactions. *J. Chem. Theory Comput.* **10**, 49–57 (2014).

32. Hobza, P., Selzle, H. L. & Schlag, E. W. Potential energy surface for the benzene dimer. Results of *ab initio* CCSD(T) calculations show two nearly isoenergetic structures: T-shaped and parallel displaced. *J. Phys. Chem.* **100**, 18790–18794 (1996).

33. Shaw, R. A. & Hill, J. G. Midbond basis functions for weakly bound complexes. *Mol. Phys.* **116**, 1460–1470 (2018).

34. Helgaker, T., Klopper, W., Koch, H. & Noga, J. Basis-set convergence of correlated calculations on water. *J. Chem. Phys.* **106**, 9639–9646 (1997).

35. Steele, R. P., DiStasio, R. A. & Head-Gordon, M. Non-covalent interactions with dual-basis methods: Pairings for augmented basis sets. *J. Chem. Theory Comput.* **5**, 1560–1572 (2009).

36. Kodrycka, M. & Patkowski, K. Platinum, gold and silver standards of intermolecular energy calculations. *J. Chem. Phys.* **151**, 070901 (2019).

37. Řezáč, J. & Hobza, P. Benchmark calculations of interaction energies in noncovalent complexes and their applications. *Chem. Rev.* **116**, 5038–5071 (2016).

38. Marshall, M. S., Burns, L. A. & Sherrill, C. D. Basis set convergence of the coupled-cluster correction, $\delta_{\text{mp2}}^{\text{ccsd(t)}}$: Best practices for benchmarking non-covalent interactions and attendant revision of the S22, NBC10, HBC6 and HSG databases. *J. Chem. Phys.* **135**, 194102 (2011).

39. Knizia, G., Adler, T. B. & Werner, H.-J. Simplified CCSD(T)-F12 methods: Theory and benchmarks. *J. Chem. Phys.* **130**, 054104 (2009).

40. Adler, T. B., Knizia, G. & Werner, H.-J. A simple and efficient CCSD(T)-F12 approximation. *J. Chem. Phys.* **127**, 221106 (2007).

41. Patkowski, K. Basis set converged weak interactions from conventional and explicitly correlated coupled-cluster approach. *J. Chem. Phys.* **138**, 154101 (2013).

42. Sirianni, D. A., Burns, L. A. & Sherrill, C. D. Comparison of explicitly correlated methods for computing high-accuracy benchmark energies for noncovalent interactions. *J. Chem. Theory Comput.* **13**, 86–99 (2017).

43. Marshall, M. S., Sears, J. S., Burns, L. A., Breédas, J.-L. & Sherrill, C. D. An error and efficiency analysis of approximations to Møller-Plesset perturbation theory. *J. Chem. Theory Comput.* **6**, 3681–3687 (2010).

44. Weigend, F. A fully direct RI-HF algorithm: Implementation, optimised auxiliary basis sets, demonstration of accuracy and efficiency. *Phys. Chem. Chem. Phys.* **4**, 4285–4291 (2002).

45. Weigend, F., Köhn, A. & Hättig, C. Efficient use of the correlation consistent basis sets in resolution of the identity MP2 calculations. *J. Chem. Phys.* **116**, 3175–3183 (2002).

46. Peterson, K. A. & Dunning, T. H. Accurate correlation consistent basis sets for molecular core-valence correlation effects: The second row atoms Al-Ar and the first row atoms B-Ne revisited. *J. Chem. Phys.* **117**, 10548–10560 (2002).

47. Trail, J. R. & Needs, R. J. Shape and energy consistent pseudopotentials for correlated electron systems. *J. Chem. Phys.* **146**, 204107 (2017).

48. Ripplinger, C., Sanhoefer, B., Hansen, A. & Neese, F. Natural triple excitations in local coupled cluster calculations with pair natural orbitals. *J. Chem. Phys.* **139**, 134101 (2013).

49. Nagy, P. R., Samu, G. & Kállay, M. Optimization of the linear-scaling local natural orbital CCSD(T) method: Improved algorithm and benchmark applications. *J. Chem. Theory Comput.* **14**, 4193–4215 (2018).

50. Ma, Q. & Werner, H.-J. Explicitly correlated local coupled-cluster methods using pair natural orbitals. *WIREs Comput. Mol. Sci.* **8**, e1371 (2018).

51. Nagy, P. R. State-of-the-art local correlation methods enable affordable gold standard quantum chemistry for up to hundreds of atoms. *Chem. Sci.* **15**, 14556–14584 (2024).

52. Hansen, A., Knowles, P. J. & Werner, H.-J. Accurate calculation of noncovalent interactions using PNO-LCCSD(T)-F12 in Molpro. *J. Phys. Chem. A* **129**, 4812–4833 (2025).

53. Jakubikova, E., Rappé, A. K. & Bernstein, E. R. Exploration of basis set issues for calculation of intermolecular interactions. *J. Phys. Chem. A* **110**, 9529–9541 (2006).

54. Hill, J. G., Platts, J. A. & Werner, H.-J. Calculation of intermolecular interactions in the benzene dimer using coupled-cluster and local electron correlation methods. *Phys. Chem. Chem. Phys.* **8**, 4072–4078 (2006).

55. Krause, C. & Werner, H.-J. Comparison of explicitly correlated local coupled-cluster methods with various choices of virtual orbitals. *Phys. Chem. Chem. Phys.* **14**, 7591–7604 (2012).

56. Altun, A., Ghosh, S., Ripplinger, C., Neese, F. & Bistoni, G. Addressing the system-size dependence of the local approximation error in coupled-cluster calculations. *J. Phys. Chem. A* **125**, 9932–9939.

57. Ma, Q. & Werner, H.-J. Scalable electron correlation methods. 5. Parallel perturbative triples correction for explicitly correlated local coupled cluster with pair natural orbitals. *J. Chem. Theory Comput.* **14**, 198–215 (2018).

58. Hampel, C. & Werner, H.-J. Local treatment of electron correlation in coupled cluster theory. *J. Chem. Phys.* **104**, 16 (1996).

59. Saebø, S., Tong, W. & Pulay, P. Efficient elimination of basis set superposition errors by the local correlation method: Accurate *ab initio* studies of the water dimer. *J. Chem. Phys.* **98**, 2170–2175 (1993).

60. Runeberg, N., Schütz, M. & Werner, H.-J. The aurophilic attraction as interpreted by local correlation methods. *J. Chem. Phys.* **110**, 7210–7215 (1999).

61. Schütz, M., Rauhut, G. & Werner, H.-J. Local treatment of electron correlation in molecular clusters: Structures and stabilities of $(\text{H}_2\text{O})_n$, $n = 2\text{--}4$. *J. Phys. Chem. A* **102**, 5997–6003 (1998).

62. Sorathia, K. & Tew, D. P. Basis set extrapolation in pair natural orbital theories. *J. Chem. Phys.* **153**, 174112 (2020).

63. Demovičová, L., Hobza, P. & Řezáč, J. Evaluation of composite schemes for CCSDT(Q) calculations of interaction energies of noncovalent complexes. *Phys. Chem. Chem. Phys.* **16**, 19115–19121 (2014).

64. Semidalas, E., Boese, A. D. & Martin, J. M. L. Post-CCSD(T) corrections in the S66 noncovalent interactions benchmark. *Chem. Phys. Lett.* **836**, 141874 (2025).

65. Shepherd, J. J. & Grüneis, A. Many-body quantum chemistry for the electron gas: Convergent perturbative theories. *Phys. Rev. Lett.* **110**, 226401 (2013).

66. Shen, B., Tatchen, J., Sanchez-Garcia, E. & Bettinger, H. F. Evolution of the optical gap in the acene series: Undecacene. *Angew. Chem. Int. Ed.* **130**, 10537–10931 (2018).

67. Tönshoff, C. & Bettinger, H. F. Pushing the limits of acene chemistry: The recent surge of large acenes. *Chem. Eur. J.* **27**, 3187–3569 (2020).

68. Novoselov, K. S. *et al.* Electronic field effect in atomically thin carbon films. *Science* **306**, 666–669 (2004).

69. Rickert, C., Usyat, D. & Kats, D. Tensor decomposed distinguishable cluster. I. Triples decomposition. *J. Chem. Phys.* **163**, 064103 (2025).

70. Kats, D. The distinguishable cluster approximation. II. The role of orbital relaxation. *J. Chem. Phys.* **141**, 061101 (2014).

71. Kats, D. & Manby, F. R. The distinguishable cluster approximation. *J. Chem. Phys.* **139**, 021102 (2013).

72. Kats, D. & Köhn, A. On the distinguishable cluster approximation for triple excitations. *J. Chem. Phys.* **150**, 151101 (2019).

73. Řezáč, J., Dubecký, M., Jurečka, P. & Hobza, P. Extensions and applications of the A24 dataset of accurate interaction energies. *Phys. Chem. Chem. Phys.* **17**, 19268–19277 (2015).

74. Lambie, S., Rickert, C., Kats, D., Usyat, D. & Alavi, A. Benchmarking distinguishable cluster methods to platinum standard CCSDT(Q) non covalent interaction energies in the A24 dataset. *arXiv* 2505.08483 (2025).

75. Smith, D. G. A., Slawik, P. J. M., Witek, H. & Patkowski, K. Basis set convergence of the post-CCSD(T) contribution to noncovalent interaction energies. *J. Chem. Theory Comput.* **10**, 3140–3150 (2014).

76. Karton, A. & Martin, J. M. L. Prototypical $\pi - \pi$ dimers re-examined by means of high-level CCSDT(Q) composite *ab initio* methods. *J. Chem. Phys.* **154**, 124117 (2021).

77. Needs, R. J., Towler, M. D., Drummond, N. D., López Ríos, P. & Trail, J. R. Variational and diffusion quantum Monte Carlo calculations with the CASINO code. *J. Chem. Phys.* **152**, 154106 (2020).

78. Dubecký, M., Jurečka, P., Mitas, L., Ditte, M. & Fanta, R. Toward accurate hydrogen bonds by scalable quantum monte carlo. *J. Chem. Theory Comput.* **15**, 3552–3557 (2019).

79. Filippi, C. & Umrigar, C. J. Multiconfiguration wave functions for quantum Monte Carlo calculations of first-row diatomic molecules. *J. Chem. Phys.* **105**, 213–226 (1996).

80. Brown, M. D., Trail, J. R., López Ríos, P. & Needs, R. J. Energies of the first row atoms from quantum Monte Carlo. *J. Chem. Phys.* **126**, 224110 (2007).

81. Seth, P., López Ríos, P. & Needs, R. J. Quantum Monte Carlo study of the first-row atoms and ions. *J. Chem. Phys.* **134**, 084105 (2011).

82. Petruzielo, F. R., Toulouse, J. & Umrigar, C. J. Approaching chemical accuracy with quantum Monte Carlo. *J. Chem. Phys.* **136**, 124116 (2012).

83. Morales, M. A., McMinis, J., Clark, B. K., Kim, J. & Scuseria, G. E. Multideterminant wave functions in quantum Monte Carlo. *J. Chem. Theory Comput.* **8**, 2181–2188 (2012).

84. Giner, E., Assaraf, R. & Toulouse, J. Quantum Monte Carlo with reoptimised perturbatively selected configuration-interaction wave functions. *Mol. Phys.* **114**, 910–920 (2016).

85. Scemama, A., Benali, A., Jacquemin, D., Caffarel, M. & Loos, P.-F. Excitation energies from diffusion Monte Carlo using selected configuration interaction nodes. *J. Chem. Phys.* **149**, 034108 (2018).

86. Scemama, A., Caffarel, M., Benali, A., Jacquemin, D. & Loos, P.-F. Influence of pseudopotentials on excitation energies from selected configuration interaction and diffusion Monte Carlo. *Results Chem.* **1**, 100002 (2019).

87. Dash, M., Moroni, S., Scemama, A. & Filippi, C. Perturbatively selected configuration-interaction wave functions for efficient geometry optimization in quantum Monte Carlo. *J. Chem. Theory Comput.* **14**, 4176–4182 (2018).

88. Dash, M., Feldt, J., Moroni, S., Scemama, A. & Filippi, C. Excited states with selected configuration interaction-quantum Monte Carlo: Chemically accurate excitation energies and geometries. *J. Chem. Theory Comput.* **15**, 4896–4906 (2019).

89. Dash, M., Moroni, S., Filippi, C. & Scemama, A. Tailoring CIPSI expansions for QMC calculations of electronic excitations: The case study of thiophene. *J. Chem. Theory Comput.* **17**, 3426–3434 (2021).

90. Feynman, R. P. & Cohen, M. Energy spectrum of the excitations in liquid helium. *Phys. Rev.* **102**, 1189–1204 (1956).

91. Lee, M. A., Schmidt, K. E., Kalos, M. H. & Chester, G. V. Green's function Monte Carlo method for liquid ${}^3\text{He}$. *Phys. Rev. Lett.* **46**, 728–731 (1981).

92. Kwon, Y., Ceperley, D. M. & Martin, R. M. Effects of backflow correlation in the three-dimensional electron gas: Quantum Monte Carlo study. *Phys. Rev. B* **58**, 6800–6806 (1998).

93. Holzmann, M., Ceperley, D. M., Pierleoni, C. & Esler, K. Backflow correlations for the electron gas and metallic hydrogen. *Phys. Rev. E* **68**, 046707 (2003).

94. López Ríos, P., Ma, A., Drummond, N. D., Towler, M. D. & Needs, R. J. Inhomogeneous backflow transformations in quantum Monte Carlo calculations. *Phys. Rev. E* **74**, 066701 (2006).

95. Pfau, D., Spencer, J. S., Matthews, A. G. D. G. & Foulkes, W. M. C. Ab initio solution of the many-electron Schrödinger equation with deep neural networks. *Phys. Rev. Res.* **2**, 033429 (2020).

96. Hermann, J., Schätzle, Z. & Noé, F. Deep-neural-network solution of the electronic schrödinger equation. *Nat. Chem.* **12**, 891 (2020).

97. Haupt, J. P. *et al.* Optimizing Jastrow factors for the transcorrelated method. *J. Chem. Phys.* **158**, 224105 (2023).

98. Filip, M.-A. *et al.* Deterministic optimization of Jastrow factors. *J. Chem. Phys.* **163**, 084107 (2025).

99. Spink, G. G., López Ríos, P., Drummond, N. D. & Needs, R. J. Trion formation in a two-dimensional hole-doped electron gas. *Phys. Rev. B* **94**, 041410 (2016).

100. Řezáč, J. *et al.* Quantum chemical benchmark energy and geometry database for molecular clusters and complex molecular systems (begdb.org): A users manual and examples. *Collect. Czech. Chem. Commun.* **73**, 1261–1270 (2008).

101. Werner, H.-J. *et al.* Molpro: A general-purpose quantum chemistry program package. *WIREs Comput. Mol. Sci.* **2**, 242–253 (2012).

102. Werner, H.-J. *et al.* The Molpro quantum chemistry package. *J. Chem. Phys.* **152**, 144107 (2020).

103. Dunning Jr., T. H. Gaussian basis sets for use in correlated molecular calculations. I. The atoms boron through neon and hydrogen. *J. Chem. Phys.* **90**, 1007–1023 (1989).

104. Werner, H.-J. & Hansen, A. Accurate calculation of isomerization and conformational energies of larger molecules using explicitly correlated local coupled cluster methods in Molpro and ORCA. *J. Chem. Theory Comput.* **19**, 7007–7030 (2023).

105. Rishi, V. & Valeev, E. F. Can the distinguishable cluster approximation be improved systematically by including connected triples? *J. Chem. Phys.* **151**, 064102 (2019).

106. Schraivogel, T. & Kats, D. Accuracy of the distinguishable cluster approximation for triple excitations for open-shell molecules and excited states. *J. Chem. Phys.* **155**, 064101 (2021).

107. Hino, O., Kinoshita, T. & Bartlett, R. J. Singular value decomposition applied to the compression of t_3 amplitude for the coupled cluster method. *J. Chem. Phys.* **121**, 1206–1213 (2004).

108. Kinoshita, T., Hino, O. & Bartlett, R. J. Singular value decomposition approach for the approximate coupled-cluster method. *J. Chem. Phys.* **119**, 7756–7762 (2003).

109. Lesiuk, M. Implementation of the coupled-cluster method with single, double and triple excitations using tensor decomposition. *J. Chem. Theory Comput.* **16**, 453–467 (2020).

110. Kats, D., Schraivogel, T., Hauskrecht, J., Rickert, C. & Wu, F. ElemCo.jl: Julia program package for electron correlation methods (2024).

111. Casula, M. Beyond the locality approximation in the standard diffusion Monte Carlo method. *Phys. Rev. B* **74**, 161102 (2006).

112. Casula, M., Moroni, S., Sorella, S. & Filippi, C. Size-consistent variational approaches to nonlocal pseudopotentials: Standard and lattice regularized diffusion Monte Carlo methods revisited. *J. Chem. Phys.* **132**, 154113 (2010).

113. Zen, A., Sorella, S., Gillan, M. J., Michaelides, A. & Alfè, D. Boosting the accuracy and speed of quantum Monte Carlo: Size consistency and time step. *Phys. Rev. B* **93**, 241118 (2016).

114. Lee, R. M., Conduit, G. J., Nemeć, N., López Ríos, P. & Drummond, N. D. Strategies for improving the efficiency of quantum Monte Carlo calculations. *Phys. Rev. E* **83**, 066706 (2011).

115. Vrbik, J. & Rothstein, S. M. Optimal spacing and weights in diffusion Monte Carlo. *Int. J. Quantum Chem.* **29**, 461–468 (1986).

116. Alfè, D. & Gillan, M. J. Efficient localized basis set for quantum Monte Carlo calculations on condensed matter. *Phys. Rev. B* **70**, 161101 (2004).

117. Ma, A., Towler, M. D., Drummond, N. D. & Needs, R. J. Scheme for adding electron–nucleus cusps to Gaussian orbitals. *J. Chem. Phys.* **122**, 224322 (2005).
118. López Ríos, P., Seth, P., Drummond, N. D. & Needs, R. J. Framework for constructing generic Jastrow correlation factors. *Phys. Rev. E* **86**, 036703 (2012).
119. Drummond, N. D., Towler, M. D. & Needs, R. J. Jastrow correlation factor for atoms, molecules, and solids. *Phys. Rev. B* **70**, 235119 (2004).
120. Toulouse, J. & Umrigar, C. J. Optimization of quantum Monte Carlo wave functions by energy minimization. *J. Chem. Phys.* **126**, 084102 (2007).
121. Umrigar, C. J., Toulouse, J., Filippi, C., Sorella, S. & Hennig, R. G. Alleviation of the fermion-sign problem by optimization of many-body wave functions. *Phys. Rev. Lett.* **98**, 110201 (2007).
122. Schmidt, K. E. & Moskowitz, J. W. Correlated Monte Carlo wave functions for the atoms He through Ne. *J. Chem. Phys.* **93**, 4172–4178 (1990).

Acknowledgments

Financial support from the Max-Planck Society is gratefully acknowledged.

Author contributions statement

S.L. was responsible for the coupled cluster calculations. P.L.R. was responsible for the diffusion Monte Carlo calculations. D.K. oversaw the coupled cluster calculations and provided software implementation for SVD-DC-CCSDT+ calculations. A.A. supervised the project. All authors discussed the results and contributed to the preparation of the manuscript. All authors have approved the final manuscript.

Competing interests

The authors have no competing interests to declare.

Supplementary Information: Nodal error behind discrepancies
between coupled cluster and diffusion Monte Carlo in
hydrogen-bonded systems

S. Lambie¹, P. López Ríos¹, D. Kats¹, and A. Alavi^{1,2,*}

¹Max Planck Institute for Solid State Research, Heisenbergstraße 1, 70569 Stuttgart, Germany

²Yusuf Hamied Department of Chemistry, University of Cambridge, Lensfield Road, Cambridge CB2 1EW, United Kingdom

*Email: a.alavi@fkf.mpg.de

January 22, 2026

S1 Additional coupled cluster results

Table S1: Density-fitted (DF) and heavy-atom only augmented (HA) CCSD(T) interaction energies for the AcOH dimer. 0.5CP-corrected results are reported, with the error being one half of the total CP correction.

In text-referral	Treatment	E_{int} [kcal mol ⁻¹]
DF-CCSD(T)	HF/DF-aV5Z + MP2/DF-aV{Q,5}Z + $\Delta\text{CCSD(T)}/aV\{T,Q\}Z$	-19.41(5)
HA-CCSD(T)	HF/aVQZ+ CCSD(T)/haV{T,Q}Z	-19.42(2)

Heavy atom augmented basis sets/HA-CCSD(T)

A widely-employed basis set in the calculation of non-covalent interactions is the so-called ‘heavy atom augmented basis set’ whereby augmentation functions are removed from the H atom basis sets, with reportedly minimal effect on the interaction energies.¹ Here, we show results that support this for the AcOH dimer.

Density fitted basis sets/FP-CCSD(T)

Density fitting (DF) is often used to reduce the memory and increase the speed of quantum chemical calculations. For all density fitted calculations carried out in this work, the JKFIT² and MPFIT³ basis sets are used are at same cardinal number as the atomic orbital basis set.

S2 VMC and DMC calculations

S2.1 Trial wave functions and optimization

Our basic trial wave function is of the Slater-Jastrow (SJ) form,

$$\Psi_{\text{SJ}}(\mathbf{R}) = e^{J(\mathbf{R})} \Psi_{\text{S}}(\mathbf{R}) , \quad (1)$$

with

$$\Psi_{\text{S}}(\mathbf{R}) = \det[\phi_i(\mathbf{r}_j^\uparrow)] \det[\phi_i(\mathbf{r}_j^\downarrow)] , \quad (2)$$

where \mathbf{R} denotes the set of up- and down-spin electron position vectors $\{\mathbf{r}_j^\uparrow\}$ and $\{\mathbf{r}_j^\downarrow\}$, $\{\phi_i\}$ are spin-independent single-particle molecular orbitals and e^J is a Jastrow correlation factor. In our all-electron (AE) calculations we modify the orbitals close to the nuclei in order to impose the electron-nucleus Kato cusp conditions.⁴

S2.1.1 Jastrow factor

We use Jastrow factors including isotropic electron-electron, electron-nucleus, and electron-electron-nucleus terms,⁵

$$J = \sum_{i < j}^{N_e} u_{P_{ij}}(r_{ij}) + \sum_i^{N_e} \sum_I^{N_n} \chi_{S_{iI}}(r_{iI}) + \sum_{i < j}^{N_e} \sum_I^{N_n} f_{T_{ijI}}(r_{ij}, r_{iI}, r_{jI}) , \quad (3)$$

which are expressed as natural-power expansions in the relevant inter-particle distances,⁶

$$\begin{aligned} u_P(r_{ij}) &= t(r_{ij}, L_u) \sum_{k=0}^{n_u} a_k^{(P)} r_{ij}^k , \\ \chi_S(r_{iI}) &= t(r_{iI}, L_\chi) \sum_{k=0}^{n_\chi} b_k^{(S)} r_{iI}^k , \\ f_T(r_{ij}, r_{iI}, r_{jI}) &= t(r_{iI}, L_f) t(r_{jI}, L_f) \sum_{k,l,m=0}^{n_f} c_{klm}^{(T)} r_{ij}^k r_{iI}^l r_{jI}^m , \end{aligned} \quad (4)$$

where $n_u = 8$, $n_\chi = 8$, and $n_f = 3$ are expansion orders, $\{a\}$, $\{b\}$, and $\{c\}$ are optimizable parameters, $L_u = 4.5$, $L_\chi = 4$, and $L_f = 4$ are fixed cut-off lengths, $t(r, L) = (1-r/L)^3 \Theta_H(L-r)$ is a cut-off function, and $\Theta_H(x)$ is the Heaviside step function. Indices P_{ij} , S_{iI} , and T_{ijI} allow the use of different parameter sets for same- and opposite-spin electron pairs and for different atomic species on distinct molecules. Our Jastrow factors for the acetic acid monomer and dimer contain 196 free parameters, while those for the water, peptide, and water-peptide systems contain 136, 256, and 376 parameters, respectively.

S2.1.2 Backflow transformation

The Slater-Jastrow-backflow (SJB) wave function is of the form

$$\Psi_{\text{SJB}} = e^{J(\mathbf{R})} \Psi_{\text{S}}[\mathbf{X}(\mathbf{R})] , \quad (5)$$

where the quasiparticle coordinates $\{\mathbf{x}_i(\mathbf{R})\}$ are of the inhomogeneous form proposed by López Ríos *et al.*⁷ including electron-electron, electron-nucleus, and electron-electron-nucleus terms,

$$\mathbf{x}_i = \mathbf{r}_i + \sum_{j \neq i}^N \eta_{P_{ij}}(r_{ij}) \mathbf{r}_{ij} + \sum_I^{N_n} \mu_{S_{ij}}(r_{iI}) \mathbf{r}_{iI} + \sum_{j \neq i}^N \sum_I^{N_n} [\Phi_{T_{ijI}}(r_{ij}, r_{iI}, r_{jI}) \mathbf{r}_{ij} + \Theta_{T_{ijI}}(r_{ij}, r_{iI}, r_{jI}) \mathbf{r}_{iI}] , \quad (6)$$

which, like the functions in the Jastrow factor, are expressed as natural-power expansions in the relevant inter-particle distances,

$$\begin{aligned}
\eta_P(r) &= t_P(r, L_\eta) \sum_{k=0}^{n_\eta} c_k^{(P)} r^k, \\
\mu_S(r) &= t_S(r, L_\mu) \sum_{k=0}^{n_\mu} d_k^{(S)} r^k, \\
\Phi_T(r_{ij}, r_{iI}, r_{iJ}) &= t_T(r_{iI}, L_\Phi) t_T(r_{jI}, L_\Phi) \sum_{k,l,m=0}^{n_\Phi} \phi_{klm}^{(T)} r_{ij}^k r_{iI}^l r_{jI}^m, \\
\Theta_T(r_{ij}, r_{iI}, r_{iJ}) &= t_T(r_{iI}, L_\Phi) t_T(r_{jI}, L_\Phi) \sum_{k,l,m=0}^{n_\Phi} \theta_{klm}^{(T)} r_{ij}^k r_{iI}^l r_{jI}^m,
\end{aligned} \tag{7}$$

where $n_\eta = 8$, $n_\mu = 8$, and $n_\Phi = 2$ are expansion orders, $\{c\}$, $\{d\}$, $\{\phi\}$, and $\{\theta\}$ are optimizable parameters, and $L_\eta = 4$, $L_\mu = 4.5$, and $L_\Phi = 4.5$ are fixed cut-off lengths. Our backflow functions the acetic acid monomer and dimer contain 230 free parameters, while those for the water, peptide, and water-peptide systems contain 295, 557, and 819 parameters, respectively.

S2.1.3 Wave function optimization

We have optimized all of our wave functions using linear least-squares energy minimization^{8,9} using a correlated-sampling approach with n_{opt} VMC-generated real-space configurations. For the acetic acid monomer and dimer, and for the water, peptide, and water-peptide systems we have used $n_{\text{opt}} = 10^6$ for Slater-Jastrow wave functions. As detailed in Section S2.3, our Slater-Jastrow-backflow wave functions have been optimized with a number of configurations chosen so as to keep the optimization uncertainty under a threshold; we have used $n_{\text{opt}} = 10^7$ for the acetic acid monomer and dimer, and $n_{\text{opt}} = 10^7$, 10^6 , and 7.5×10^6 respectively for the water, peptide, and water-peptide systems.

S2.2 DMC calculation details

S2.2.1 DMC time step convergence of SJ-DMC results

Time-step bias is a smooth function of the DMC time step which is linear in τ as $\tau \rightarrow 0$, and it is often negligible in energy differences due to cancellation of errors. However care must be taken to verify the range of linearity and/or the degree of cancellation on a case-by-case basis, noting that the choice of localization scheme significantly affects time-step dependence.

We have chosen to use the T-move localization scheme in our calculations to avoid the beyond-first-order behavior seen for the determinant localization approximation (DLA) in the time-step bias plots of the supplementary information of Ref. 10. It should be noted that for all systems in the S66 set, the “typical” time-step range of $\tau = 0.01\text{--}0.04$ a.u. suggested for ECP systems in Ref. 11 appears falls outside the regime where total energies can be regarded to be linear functions of τ , and therefore this range suggestion should not be followed blindly when the DLA scheme is used.

In Fig. S1 we plot the time-step dependence of the total DMC energies obtained for the AcOH monomer and dimer, and Fig. S2 shows the time-step dependence of the total DMC energies obtained for the water, peptide, and water-peptide systems. Our ECP SJ-DMC and ECP SJB-DMC results have been obtained by linear extrapolation to zero time step of the energies obtained at $\tau = 0.004$ and 0.016 a.u., for efficiency,^{12,13} and these energies and fits are shown in Figs. S1 and S2, along with additional DMC energies at other time steps to provide visual confirmation that the ECP DMC energy is linear in the time step for the ECP systems.

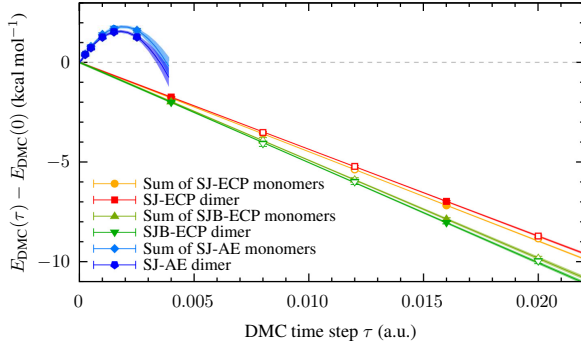


Figure S1: Time-step bias on the ECP SJ-DMC and ECP SJB-DMC total energy of the AcOH dimer and on twice the total energy of the AcOH monomer, along with AE SJ-DMC results for comparison. Solid symbols represent data points used in the corresponding fits, while open symbols are ignored in fits and shown to verify linear trends only. Lines represent fits to the data, and shaded areas around them represent 95% confidence intervals on the fit values, while errorbars represent 95% confidence intervals around data points.

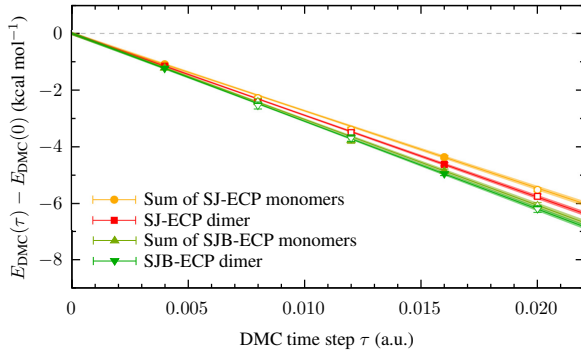


Figure S2: Time-step bias on the ECP SJ-DMC and ECP SJB-DMC total energy of the water-peptide system and on the sum of the total energies of the water and peptide monomers. Solid symbols represent data points used in the corresponding fits, while open symbols are ignored in fits and shown to verify linear trends only. Lines represent fits to the data, and shaded areas around them represent 95% confidence intervals on the fit values, while errorbars represent 95% confidence intervals around data points.

Note that the time steps for our ECP calculations were chosen so that DMC energies using the DLA scheme, should we have chosen to run them, would have been linearly extrapolatable to zero time step; if we had targeted the T-move scheme alone from the outset we should have been able to use significantly larger time steps.

For the AcOH monomer and dimer, Fig. S1 also shows AE SJ-DMC energies, which we extrapolate to zero time step by fitting all five data points to a second-order polynomial, and we use this result to test the accuracy of the ECP approximation. The two-point linear extrapolation of the ECP SJ-DMC results gives an interaction energy of $-20.13(6)$ kcal mol $^{-1}$, within uncertainty of the quadratic extrapolation of the AE SJ-DMC energies of $-20.29(16)$ kcal mol $^{-1}$, and we conclude that the ECP approximation does not introduce a significant error.

S2.2.2 DMC population control bias

We have used a target DMC population of 65536 walkers at the smallest time step for each system, and have kept the population proportional to $1/\tau$ at other time steps in order to remove the (likely negligible) population control bias from our results.¹¹

S2.3 SJB-DMC optimization uncertainty

The uncertainty introduced by the stochastic optimization of wave function parameters is typically ignored in VMC and DMC calculations. This is partly justified in some cases: the error in the VMC energy is quadratic in the error in the optimized parameter set when energy minimization is used, while the SJ-DMC energy of all-electron systems at zero time step is independent of the parameter values. However VMC energies of variance-minimized wave functions,^{14,15} VMC expectation values of operators other than the Hamiltonian,¹⁶ and beyond-SJ DMC energies are affected by errors linear in the error in the optimized parameter set; obtaining accurate values for these requires converging the results with respect to sample size.^{14,15}

S2.3.1 Dependence of the optimization uncertainty on the VMC-based optimization sample size

In correlated-sampling optimization, one generates n_{opt} random real-space electronic configurations $\{\mathbf{R}_i\}_{i=1}^{n_{\text{opt}}}$ distributed according to an initial wave function $\Psi(\mathbf{p}; \mathbf{R})$, where \mathbf{p} are the wave function parameters. The local energy is evaluated at these configurations, $E_L(\mathbf{p}, \mathbf{R}_i) = \Psi^{-1}(\mathbf{p}, \mathbf{R}_i) \hat{H}(\mathbf{R}_i) \Psi(\mathbf{p}, \mathbf{R}_i)$, and the resulting VMC energy $E_{\text{VMC}}(\mathbf{p})$ is computed as the average of the local energies, which has a standard error proportional to $n_{\text{opt}}^{-1/2}$. The variational energy is then minimized by varying \mathbf{p} while keeping the configurations $\{\mathbf{R}_i\}_{i=1}^{n_{\text{opt}}}$ fixed. The optimizer will clearly only be able to locate the parameters that minimize the variational energy to the degree that the statistical uncertainty on the variational energy allows, and thus the the parameter set \mathbf{p}' resulting from the optimization procedure is a random vector which follows a probability distribution of spread determined by that of the variational energy. At sufficiently large sample sizes, the central limit theorem applies to both $E_{\text{VMC}}(\mathbf{p})$ and \mathbf{p}' , and by error propagation to leading order, the uncertainty on \mathbf{p}' is proportional to that in $E_{\text{VMC}}(\mathbf{p})$, which in turn makes it proportional to $n_{\text{opt}}^{-1/2}$.

The DMC energy is a function of the optimized wave function parameters, $E_{\text{DMC}}(\mathbf{p}')$, and again by error propagation to leading order, the contribution from the uncertainty on \mathbf{p}' to the uncertainty on $E_{\text{DMC}}(\mathbf{p}')$ is proportional to $n_{\text{opt}}^{-1/2}$. Thus, the optimization uncertainty on the SJB-DMC energy is indirectly dependent on the number of real-space configurations n_{opt} used in the VMC-based correlated-sampling optimization process.

S2.3.2 Evaluating the optimization uncertainty

The most direct, brute-force way of obtaining the optimization uncertainty, σ_{opt} , for any given system is to perform multiple independent random instances of wave function optimization each followed by a DMC run, and evaluating σ_{opt} as the standard deviation of the resulting DMC energies. For the systems in this work we perform 20 such independent random instances, and we perform a single DMC run at $\tau = 0.016$ a.u. under the assumption that σ_{opt} is independent of time step, which we verify below.

In order to ascertain that σ_{opt} is a well-behaved function of n_{opt} , we have evaluated the optimization uncertainty of the AcOH monomer, $\sigma_{\text{opt}}^{\text{AcOH}}$, at each of four sample sizes n_{opt} ranging between 10^4 and 10^6 . Given that the interaction between the AcOH monomers in the dimer is weak, we take the optimization uncertainty for the AcOH dimer, $\sigma_{\text{opt}}^{(\text{AcOH})_2}$, to be very $\sqrt{2}$ times that of the monomer at the same n_{opt} . We have verified this at $n_{\text{opt}} = 10^5$, where we obtain an uncertainty ratio of $\sigma_{\text{opt}}^{(\text{AcOH})_2}/\sigma_{\text{opt}}^{\text{AcOH}} = 1.72 \pm 0.54$, which well within one standard deviation from $\sqrt{2}$. We take the total optimization uncertainty on the interaction energy of the AcOH dimer to be $\sigma_{\text{opt}} = \sqrt{(2\sigma_{\text{opt}}^{\text{AcOH}})^2 + \sigma_{\text{opt}}^{(\text{AcOH})_2}^2} = \sqrt{6}\sigma_{\text{opt}}^{\text{AcOH}}$, so our target optimization uncertainty for the interaction energy of $\sigma_{\text{opt}} = 0.071$ kcal mol⁻¹ translates into a target $\sigma_{\text{opt}}^{\text{AcOH}} \approx 0.029$ kcal mol⁻¹.

We have also tested the time-step dependence of the optimization uncertainty by running SJB-DMC calculations at $\tau = 0.004$ a.u. for each of the 20 SJB wave functions optimized at $n_{\text{opt}} = 10^5$, and we plot the corresponding linear extrapolations in Fig. S3. The standard deviation of the SJB-DMC energies extrapolated to $\tau = 0$ is 0.14 kcal mol $^{-1}$, which is about half that at $\tau = 0.016$ a.u. of 0.26 kcal mol $^{-1}$. We conclude that approximating the optimization uncertainty at $\tau = 0$ by the value obtained at $\tau = 0.016$ a.u. provides a safe overestimation of its true value, and we apply this approximation throughout.

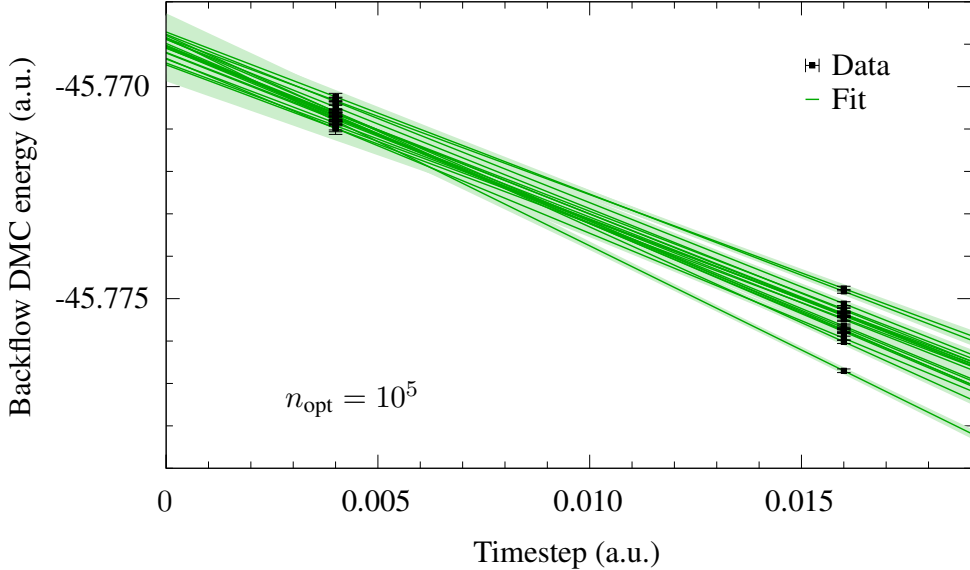


Figure S3: ECP SJB-DMC energy as a function of time step for 20 independent random instances of wave function optimization at sample size $n_{\text{opt}} = 10^5$. Lines are linear fits to the data, and shaded areas around them represent 95% confidence intervals on fit values, while errorbars represent 95% confidence intervals around data points.

We compute the optimization sample size by linear extrapolation in log-log scale using the formula $\log \sigma_{\text{opt}} = \alpha - 1/2 \log n_{\text{opt}}$. For the AcOH molecule we perform a least-squares fit to this formula using the result from all four sample sizes, and for other systems where we only perform tests at $n_{\text{opt}} = 30\,000$ we simply substitute the values of σ_{opt} and n_{opt} into the formula and solve for α .

For the AcOH monomer and dimer we use $n_{\text{opt}} = 10^7$, which yields an optimization uncertainty on the interaction energy at $n_{\text{opt}} = 10^7$ of $\sigma_{\text{opt}} = 0.060$ kcal mol $^{-1}$, below our target of 0.071 kcal mol $^{-1}$. For the water, peptide, and water-peptide systems we use $n_{\text{opt}} = 10^7$, 10^6 , and 7.5×10^6 , which yield optimization uncertainties on the total energies of 0.023 , 0.042 , and 0.049 kcal mol $^{-1}$, respectively, and an optimization uncertainty on the interaction energy of $\sigma_{\text{opt}} = 0.069$ kcal mol $^{-1}$, again below our target of 0.071 kcal mol $^{-1}$.

S3 Geometries

AcOH dimer

16

C	-1.061709204	1.297140572	0.292060003
O	-0.358161116	2.270458613	0.531812668
O	-0.589303516	0.094917758	0.003788813
H	0.404435659	0.127722621	0.018411838
C	-2.558427798	1.342549823	0.296257320
H	-2.895997978	2.347464002	0.518316340
H	-2.932889278	1.022390451	-0.672995551
H	-2.937211960	0.644910433	1.039557084
C	2.789348447	1.108419242	0.271183758
O	2.085730082	0.135104754	0.031396156
O	2.316922113	2.310854630	0.558962229
H	1.323133573	2.277956396	0.544561725
C	4.286060895	1.062516496	0.269219363
H	4.623640459	0.061197303	0.031693868
H	4.667559440	1.772869435	-0.460249535
H	4.657577206	1.365211013	1.245274724

Water-peptide

15

O	-0.392018453	-0.384718737	0.076071325
H	-0.911460851	0.413812040	0.177648774
H	0.524903820	-0.068484694	0.090511364
C	2.197705212	-2.245403490	-0.230313251
H	2.847668055	-3.106515367	-0.363228638
H	1.516729242	-2.167931431	-1.074178526
H	1.584688314	-2.384199477	0.656695112
C	2.952437290	-0.947390613	-0.097719744
O	2.375721843	0.127904243	0.058868998
N	4.303070413	-1.044893297	-0.162337713
H	4.704022041	-1.955427276	-0.291852811
C	5.171312525	0.107077163	-0.052894631
H	4.534818395	0.975377606	0.081889976
H	5.836902032	0.015621965	0.803198250
H	5.765778248	0.236497652	-0.955153818

References

- [1] Marshall, M. S.; Sears, J. S.; Burns, L. A.; Breédas, J.-L.; Sherrill, C. D. An error and efficiency analysis of approximations to Møller-Plesset perturbation theory. *J. Chem. Theory Comput.* **2010**, 6, 3681–3687.
- [2] Weigend, F. A fully direct RI-HF algorithm: Implementation, optimised auxiliary basis sets, demonstration of accuracy and efficiency. *Phys. Chem. Chem. Phys.* **2002**, 4, 4285–4291.
- [3] Weigend, F.; Köhn, A.; Hättig, C. Efficient use of the correlation consistent basis sets in resolution of the identity MP2 calculations. *J. Chem. Phys.* **2002**, 116, 3175–3183.
- [4] Ma, A.; Towler, M. D.; Drummond, N. D.; Needs, R. J. Scheme for adding electron–nucleus cusps to Gaussian orbitals. *J. Chem. Phys.* **2005**, 122, 224322.
- [5] López Ríos, P.; Seth, P.; Drummond, N. D.; Needs, R. J. Framework for constructing generic Jastrow correlation factors. *Phys. Rev. E* **2012**, 86, 036703.
- [6] Drummond, N. D.; Towler, M. D.; Needs, R. J. Jastrow correlation factor for atoms, molecules, and solids. *Phys. Rev. B* **2004**, 70, 235119.
- [7] López Ríos, P.; Ma, A.; Drummond, N. D.; Towler, M. D.; Needs, R. J. Inhomogeneous backflow transformations in quantum Monte Carlo calculations. *Phys. Rev. E* **2006**, 74, 066701.
- [8] Toulouse, J.; Umrigar, C. J. Optimization of quantum Monte Carlo wave functions by energy minimization. *J. Chem. Phys.* **2007**, 126, 084102.
- [9] Umrigar, C. J.; Toulouse, J.; Filippi, C.; Sorella, S.; Hennig, R. G. Alleviation of the Fermion-Sign Problem by Optimization of Many-Body Wave Functions. *Phys. Rev. Lett.* **2007**, 98, 110201.
- [10] Shi, B. X.; Pia, F. D.; Al-Hamdani, Y. S.; Michaelides, A.; Alfé, D.; Zen, A. Systematic discrepancies between reference methods for non-covalent interactions within the S66 dataset. *J. Chem. Phys.* **2025**, 162, 144107.
- [11] Needs, R. J.; Towler, M. D.; Drummond, N. D.; López Ríos, P.; Trail, J. R. Variational and diffusion quantum Monte Carlo calculations with the CASINO code. *J. Chem. Phys.* **2020**, 152, 154106.
- [12] Lee, R. M.; Conduit, G. J.; Nemec, N.; López Ríos, P.; Drummond, N. D. Strategies for improving the efficiency of quantum Monte Carlo calculations. *Phys. Rev. E* **2011**, 83, 066706.
- [13] Vrbik, J.; Rothstein, S. M. Optimal spacing and weights in diffusion Monte Carlo. *International Journal of Quantum Chemistry* **1986**, 29, 461–468.
- [14] Haupt, J. P.; Hosseini, S. M.; López Ríos, P.; Dobrautz, W.; Cohen, A.; Alavi, A. Optimizing Jastrow factors for the transcorrelated method. *J. Chem. Phys.* **2023**, 158, 224105.
- [15] Filip, M.-A.; Christlmaier, E. M. C.; Haupt, J. P.; Kats, D.; López Ríos, P.; Alavi, A. Deterministic optimization of Jastrow factors. *J. Chem. Phys.* **2025**, 163, 084107.
- [16] Spink, G. G.; López Ríos, P.; Drummond, N. D.; Needs, R. J. Trion formation in a two-dimensional hole-doped electron gas. *Phys. Rev. B* **2016**, 94, 041410.